

Structural and Functional Characterization of Transmembrane Segment IX of the NHE1 Isoform of the Na⁺/H⁺ Exchanger*

Received for publication, May 6, 2008, and in revised form, May 21, 2008. Published, JBC Papers in Press, May 28, 2008, DOI 10.1074/jbc.M803447200

Tyler Reddy^{†1,2}, Jie Ding^{§1,3}, Xiuju Li[§], Brian D. Sykes^{§4}, Jan K. Rainey^{†¶}, and Larry Fliegel^{§5}

From the [†]Department of Biochemistry and Molecular Biology and [¶]Department of Chemistry, Dalhousie University, Halifax, Nova Scotia B3H 1X5 and the [§]Department of Biochemistry, University of Alberta, Edmonton, Alberta T6G 2H7, Canada

The Na⁺/H⁺ exchanger isoform 1 (NHE1) is an integral membrane protein that regulates intracellular pH by removing one intracellular H⁺ in exchange for one extracellular Na⁺. It has a large N-terminal membrane domain of 12 transmembrane segments and an intracellular C-terminal regulatory domain. We characterized the cysteine accessibility of amino acids of the putative transmembrane segment IX (residues 339–363). Each residue was mutated to cysteine in a functional cysteineless NHE1 protein. Of 25 amino acids mutated, 5 were inactive or nearly so after mutation to cysteine. Several of these showed aberrant targeting to the plasma membrane and reduced expression of the intact protein, whereas others were expressed and targeted correctly but had defective NHE1 function. Of the active mutants, Glu³⁴⁶ and Ser³⁵¹ were inhibited >70% by positively charged [2- (trimethylammonium)-ethyl]methanethiosulfonate but not by anionic [2-sulfonatoethyl]methanethiosulfonate, suggesting that they are pore lining and make up part of the cation conduction pathway. Both mutants also had decreased affinity for Na⁺ and decreased activation by intracellular protons. The structure of a peptide representing amino acids 338–365 was determined by using high resolution NMR in dodecylphosphocholine micelles. The structure contained two helical regions (amino acids Met³⁴⁰–Ser³⁴⁴ and Ile³⁵³–Ser³⁵⁹) kinked with a large bend angle around a pivot point at amino acid Ser³⁵¹. The results suggest that transmembrane IX is critical with pore-lining residues and a kink at the functionally important residue Ser³⁵¹.

The mammalian Na⁺/H⁺ exchanger isoform 1 (NHE1)⁶ is a ubiquitous integral membrane protein that regulates intracellular pH by mediating removal of one intracellular proton in exchange for one extracellular sodium ion (1). NHE1 has many cellular and physiological functions. It promotes cell growth and differentiation (2), protects cells from intracellular acidification (2, 3), and also regulates sodium fluxes and cell volume after challenge by osmotic shrinkage (4). In addition, Na⁺/H⁺ exchanger activity has been demonstrated to be involved in modulating cell motility and invasiveness of neoplastic breast cancer cells (5), and it has been shown to be critical to cell motility in some cell types (6). The Na⁺/H⁺ exchanger also plays a critical causal role in heart hypertrophy and in the damage that occurs during ischemia and reperfusion. Inhibition of the exchanger with a new generation of Na⁺/H⁺ exchanger inhibitors protects the myocardium during these disease states (7–10).

NHE1 has an N-terminal membrane ion translocation domain of ~500 amino acids and a C-terminal regulatory domain of ~315 amino acids (1, 8). Wakabayashi *et al.* (11) used a combination of hydrophobicity analysis and cysteine-scanning mutagenesis to predict a topology with 3 membrane-associated segments and 12 integral transmembrane (TM) segments (Fig. 1A). A recent homology model, based on the *Escherichia coli* antiporter NhaA crystal structure (12), also predicts 12 TM segments, but assignments of transmembrane segments are different in comparison with the Wakabayashi topology (13).

The exact details of cation coordination and translocation through the central ion pore of NHE1 have only recently begun to emerge. In this respect, we have identified TM IV (14) and TM VII (15) (with topology assignments according to Ref. 11) as functionally critical. More recently, we solved the structures of these TM segments and identified specific essential residues (16, 17). Prolines 167 and 168 of TM IV were essential to NHE1 function (14) and Phe¹⁶¹ was shown to be a pore-lining residue involved in transport using cysteine-scanning mutagenesis (16). The peptide was composed of an N-terminal β -turn region, followed by an extended (nonhelical) structure

* This work was supported in part by grants from Canadian Institutes of Health Research (to L. F. and B. D. S.), from Dalhousie University, the E. Gordon Young Endowment Fund, and the Natural Sciences and Engineering Research Council of Canada (to J. K. R.). The costs of publication of this article were defrayed in part by the payment of page charges. This article must therefore be hereby marked "advertisement" in accordance with 18 U.S.C. Section 1734 solely to indicate this fact.

The atomic coordinates and structure factors (code 2k3c) have been deposited in the Protein Data Bank, Research Collaboratory for Structural Bioinformatics, Rutgers University, New Brunswick, NJ (<http://www.rcsb.org/>).

Resonance assignments have been deposited in the BioMagResBank entry 15747.

¹ Both authors contributed equally to this work.

² Supported by a Natural Sciences and Engineering Research Council Canada Graduate Scholarship (CGS-M) and recipient of critical professional development funding from the Nova Scotia Health Research Foundation.

³ Recipient of funding from the Alberta Heritage Foundation for Medical Research and from the Canadian Institutes of Health Research Strategic Training Initiative in Membrane Proteins and Cardiovascular Disease.

⁴ Recipient of support as a Canada Research Chair in Structural Biology.

⁵ Recipient of an Alberta Heritage Foundation for Medical Research Scientist award. To whom correspondence should be addressed: Dept. of Biochemistry, 347 Medical Science Bldg., University of Alberta, Edmonton, Alberta T6G 2H7, Canada. Tel.: 780-492-1848; Fax: 780-492-0886; E-mail: lfliegel@ualberta.ca.

⁶ The abbreviations used are: NHE1, Na⁺/H⁺ exchanger isoform 1; cNHE1, cysteineless NHE1; TM, transmembrane (segment); HA, hemagglutinin; MTSET ([2- (trimethylammonium)ethyl]methanethiosulfonate); MTSES ([2-sulfonatoethyl]methanethiosulfonate); NOE, nuclear Overhauser effect; NOESY, NOE spectroscopy; DPC, dodecylphosphocholine; HSQC, heteronuclear single quantum coherence spectroscopy; TOCSY, total correlation spectroscopy; r.m.s.d., root mean square deviation; DSS, (*d*₆)-2,2-dimethyl-2-silapentane-5-sulfonic acid.

TABLE 1

Oligonucleotides used for site-directed mutagenesis of TM IX

Mutated nucleotides are in lowercase letters. Mutated amino acid residues are indicated in boldface type, and new restriction sites are underlined. Restriction sites deleted are indicated in parentheses.

Mutation	Oligonucleotide sequence	Restriction site
Y339C	5'-CTTCCTTACAGCT tg CATGGCCTACTTG-3'	PvuII
M340C	5'-CCTCTACAGCTACT tg GCCTACTTGTACAGC-3'	AlwNI
A341C	5'-CAGCTACAT tg CTACTTGTTCAGC-3'	AflIII
Y342C	5'-CTACAGCTACATGGCa Tg CTTGTTCAGCCGAGC-3'	SphI
L343C	5'-GCTACATGGCCTAC Tgc agcGCCGAGCTCTCCAC-3'	PstI
S344C	5'-CATGGCCTACTTG Tg GGCaGAGCTCTCCACC-3'	FspI
A345C	5'-GGCCTACTTGT CaTg CGAaCTCTCCACCTGTC-3'	(Sacl)
E346C	5'-CTACTTGTTCAGCC tg CTCTTCCACCTGTC-3'	(Sacl)
L347C	5'-CTTGTTCAGCC gag tg CTTCCACCTGTCAG-3'	(Sacl)
F348C	5'-CTTGTTCAGCC gag CTa Tg CCaCTGTTCAGGCATC-3'	(Sacl)
H349C	5'-CAGCCGAGCTCTT tg CC Tg CTGTTCAGGCATC-3'	BglI
L350C	5'-GCCGAGCTCTTCCa tg GCagcGGCCTCATGGCGCTC-3'	PstI
S351C	5'-GCTCTTCC ac CT Tg GGCaCTCATGGCGC-3'	BstXI
G352C	5'-CTTCCACCTGT CaTg CATCATGGCGCTC-3'	NsiI
I353C	5'-CTTCCACCTGTTCAGCa tg GCATGGCGCTCATAG-3'	NsiI
M354C	5'-CACCTGTTCAGGCAT tg GGCaCTCATAGCCCTCAGG-3'	FspI
A355C	5'-CTGTTCAGGCATCAT tg CTCATAGCCCTCAGG-3'	BstAPI
L356C	5'-TCAGGCATCATGGCa tg GCATAGCCCTCAGG-3'	NsiI
I357C	5'-GCATCATGGCGCT tg GGCaCTCAGGAGTGGTGATG-3'	FspI
A358C	5'-CATGGCGCTCATA tg CTCAGGAGTGGTG-3'	NdeI
S359C	5'-CATGGCGCTCATAGCa Tg GGAGTGGTGATGCG-3'	SphI
G360C	5'-CATGGCGCTCATAGCC ag ct Gc GTGGTGATGCGCCCC-3'	PvuII
V361C	5'-CTCATAGCCCTCAGG at gt Gt CaT Ga GgCCCTATGTGGAGGC-3'	BspHI
V362C	5'-GCCTCAGGAGT tg GCATGGCCCTATG-3'	SphI
M363C	5'-GCCTCAGGAGTGGT tg CaGgCCCTATGTGGAGGC-3'	PstI

induced around Pro¹⁶⁷–Pro¹⁶⁸, and a C-terminal helical region (16). In contrast, TM VII was an interrupted helix with several residues critical for function (17). Of importance, functionally essential residues were localized at and near the flexible break point between helices.

Another important segment of the Na⁺/H⁺ exchanger is TM IX. TM IX is composed of residues 339–363 (Fig. 1B). Several studies have suggested that it is critical to NHE1 function. One study used chimeric NHEs to examine TM segments that confer sensitivity to pharmacological antagonists (18). Using hybrid NHEs of the sensitive NHE1 and resistant NHE3, TM IX was shown to be important in mediating sensitivity to the antagonists. Another study showed that alteration of His³⁴⁹ of TM IX reduced the sensitivity to amiloride compounds (19). Two other studies have shown by site-specific mutagenesis that the TM IX and Glu³⁴⁶ of TM IX are important in NHE function and drug sensitivity (20, 21).

In this study, we examine both structural and functional aspects of TM IX of the NHE1 isoform of the Na⁺/H⁺ exchanger. We use cysteine-scanning mutagenesis of TM IX in the full-length NHE1 protein to characterize which amino acids are important in function and are likely pore lining. Cysteine-scanning mutagenesis has been used to determine pore-lining residues in numerous membrane proteins (22–27), including our own study of TM IV of the Na⁺/H⁺ exchanger (16). Two sulfhydryl-reactive reagents that are often used in these studies are MTSET and MTSES, which are membrane-impermeant (28–30) and react with potentially pore-lining residues surrounded by water. Parallel structural characterization by NMR and CD spectroscopy is used to examine the structure of the TM segment in isolated peptide form. Considerable literature has suggested that the study of isolated TM segments reflects the structure and function of the intact membrane protein (31–35) especially when stabilized in membrane-mimetic dodecylphosphocholine (DPC) micelles (36, 37). Our study demon-

strates that TM IX has two helical segments and a sharp kink at a Ser³⁵¹ pivot point. Both Ser³⁵¹ and Glu³⁴⁶ appear to be critical pore-lining residues based on cysteine-scanning mutagenesis and accessibility analysis.

EXPERIMENTAL PROCEDURES

Materials—LipofectamineTM 2000 reagent was from Invitrogen, and PWO DNA polymerase was obtained from Roche Applied Science. MTSET and MTSES were from Toronto Research Chemicals, Toronto, Ontario, Canada. Deuterated DPC was purchased from C/D/N Isotopes (Pointe-Claire, Quebec, Canada).

Site-directed Mutagenesis—Mutations were made to an expression plasmid containing a tagged human NHE1 isoform of the Na⁺/H⁺ exchanger. The plasmid (pYN4+) contained the cDNA for the entire coding region of the Na⁺/H⁺ exchanger with a hemagglutinin (HA) tag that we have previously shown does not affect the function of the protein (14). The mutations made (Table 1) changed the indicated amino acids to cysteine, using the background of the functional cysteineless NHE1 protein that we have described earlier (16). Site-directed mutagenesis was done by amplification with PWO DNA polymerase (Roche Applied Science) followed by using the Stratagene (La Jolla, CA) QuikChangeTM site-directed mutagenesis kit. The mutagenesis created or deleted a restriction enzyme site for use in screening transformants. The fidelity of DNA amplification was confirmed by DNA sequencing.

Cell Culture and Transfections—Stable cell lines of all mutants were made as described earlier (14) via transfection with LipofectamineTM 2000 reagent (Invitrogen). AP-1 cells were used that lack an endogenous Na⁺/H⁺ exchanger (16). Selection was done using 800 μg/ml geneticin (G418), and stable cell lines for experiments were regularly re-established from frozen stocks at passage numbers between 5 and 9.

Characterization of TM IX of the Na⁺/H⁺ Exchanger

SDS-PAGE and Immunoblotting—Western blot analysis was used to confirm NHE1 expression (14). Cell lysates were made from stable cell lines, and equal amounts of up to 100 μg of each sample were resolved on a 10% SDS-polyacrylamide gel. Nitrocellulose transfers were immunostained using a primary antibody of anti-HA monoclonal antibody (Roche Applied Science). The secondary antibody was peroxidase-conjugated goat anti-mouse antibody (Bio/Can, Mississauga, Ontario, Canada). The Amersham Biosciences enhanced chemiluminescence blotting and detection system were used to visualize immunoreactive proteins. NIH Image 1.63 software (National Institutes of Health, Bethesda) was used for densitometric analysis of x-ray films.

Cell Surface Expression—We measured cell surface expression to ensure that all mutant proteins were properly targeted to the cell surface (14). Sulfo-NHS-SS-biotin (Pierce)-labeled cell surface proteins and immobilized streptavidin resin was used to remove plasma membrane-labeled Na⁺/H⁺ exchanger. Equal amounts of total and unbound proteins were analyzed by Western blotting against the HA tag, and densitometry was as described earlier (14). The amount of NHE1 on the cell surface was calculated by comparing both the 110- and 95-kDa immunoreactive species in Western blots of the total and unbound fractions. It was not possible to efficiently elute proteins bound to immobilized streptavidin resin reproducibly.

Na⁺/H⁺ Exchange Activity—Na⁺/H⁺ exchange activity was measured as described previously (16). Ammonium chloride was used to induce acute acid load, and the initial rate of Na⁺-induced recovery of cytosolic pH (pH_i) was measured using 2',7-bis(2-carboxyethyl)-5(6) carboxyfluorescein-AM (Molecular Probes Inc., Eugene, OR) and a PTI Deltascan spectrofluorometer. Recovery from acidosis was in the presence of 135 mM NaCl. There was no difference in the buffering capacities of the various stable cell lines. Where indicated, activity of the Na⁺/H⁺ exchanger mutants was corrected for targeting of the protein to the cell surface and for the level of protein expression. Results are the means \pm S.E., and statistical significance was determined using the Mann-Whitney *U* test.

To test the effect of MTSET and MTSES on NHE1 activity of mutants, we used the standard Na⁺/H⁺ exchanger assay with slight modification. In this case cells were acidified two times with ammonium chloride as described above. After a first control acidification and recovery, either MTSET or MTSES was added to a final concentration of 10 mM for 10 min in Na⁺-free buffer. Cells were subsequently washed three times in Na⁺-free buffer prior to the second ammonium chloride-induced acidification and recovery. To calculate residual activity during recovery from acidosis Equation 1 was used,

$$\% \text{ residual activity} = \frac{\text{pH change after (reagent)}}{\text{pH change without (reagent)}} \times 100\% \quad (\text{Eq. 1})$$

In some experiments we checked the Na⁺ and proton affinity of mutant NHE1 proteins. The determination of kinetic parameters of the Na⁺/H⁺ exchanger was essentially as described earlier (38). Na⁺ concentrations were varied while maintaining osmolarity with *N*-methyl-D-glucamine. For these experiments

cells were acidified to the same level with 50 mM NH₄Cl. To determine the proton affinity, intracellular pH was varied by acidifying to various degrees using ammonium chloride concentrations from 5 to 50 mM as described earlier (38). Buffering capacity of the cell lines was used to determine proton flux essentially as described earlier (38). Cation affinity was calculated using Sigmaplot and fitting lines to a three-parameter sigmoidal fit.

Peptide Synthesis and Purification—TM IX peptide (sequence, KSYMAYLSAELFHLGSGIMALIASGVVMPKPK; acetyl-capped N terminus, amide-capped C terminus) was purchased from GL Biochem (Shanghai, China) at >95% purity. Purity was assessed by high pressure liquid chromatography, and identity was confirmed using sequential assignment of NMR data and by matrix-assisted laser desorption ionization mass spectroscopy.

NMR Spectroscopy and Structure Calculations—The NMR sample was prepared by dissolving 0.9 \pm 0.1 mM synthetic peptide in a 95% H₂O, 5% D₂O solution containing \sim 75 mM deuterated DPC and 0.25 mM (*d*₆)-2,2-dimethyl-2-silapentane-5-sulfonic acid (DSS) for chemical shift referencing. Solution pH was adjusted to 5.05 without consideration of deuterium isotope effects, and all experiments were conducted at 30 °C. One-dimensional ¹H, natural abundance gradient-enhanced ¹H-¹³C HSQC, two-dimensional ¹H-¹H TOCSY (60-ms mix; decoupling in the presence of scalar interactions spin lock), and NOESY (225-ms mix) experiments were acquired on the Canadian National High Field NMR Centre Varian INOVA 800-MHz spectrometer. All experiments were used as configured within the Varian BioPack software package. Spectra were processed using NMRPipe (39) and analyzed using Sparky 3 (65). All spectral assignments were carried out by manual peak picking in Sparky, and resonance assignments have been deposited in the BioMagResBank (code 15747).

Structure calculations were performed in the python scripting interface of XPLOR-NIH version 2.18 (40) using NOE restraints from the assigned spectrum. Peak volumes were independently calculated using Gaussian and Lorentzian fit Sparky algorithms, with no allowed peak center motion. Those peaks that were not assigned a volume or were assigned a negative volume by the algorithm (\sim 27.5%) were either manually assigned a summed signal intensity as defined by a user-specified region or fit by Sparky algorithm after contour adjustment. Peak volumes were empirically calibrated to distance ranges of 0–5.0, 1.8–5.0, and 1.8–6.0 Å; the Lorentzian fit volumes were more conservative and used for subsequent analysis. Restraints were divided into bin ranges corresponding to strong (1.8–2.8 Å), medium (1.8–4.0 Å), weak (1.8–5.0 Å), and very weak (1.8–6.0 Å) contacts. Ambiguous assignments and NOE potential scaling were handled as described previously (17). Following 21 rounds of structural refinement by simulated annealing, an additional 6 rounds were performed with dihedral angle potential scaling factors of 5, 50, 100, 100, 50, and 25. Simulated annealing parameters were similar to those described previously (17), but with 15,000 cooling steps.

A single extended polypeptide was generated and subjected to simulated annealing for each round. To handle the families of 100 structures generated per round an in-house tcl/tk script

(freely available upon request from J. Rainey) was used; the script allowed for assessment of violations and iterative refinement of NOE restraints. Refinement gradually increased in stringency, initially violations >0.5 Å in >50% of structures were lengthened, but subsequently violations >0.1 Å in >25% of structures were modified. After 21 cycles of simulated annealing and NOE refinement, calculated XPLOR-NIH structure energies contained minimal contributions from NOE violations, and magnitudes of all observed violations were minimal. All NOE restraints were satisfied without pruning. Six further cycles of simulated annealing were carried out with incorporation of dihedral angle restraints as described above. The lowest 40 energy structures in the final ensemble of 100 were retained for further analysis. The final sets of restraints have been deposited in the Protein Data Bank with this ensemble of 40 structures (Research Collaboratory for Structural Bioinformatics Protein Data Bank code 2k3c).

CD Spectroscopy and Analysis—Samples for CD spectroscopy were diluted from the previously described NMR sample to obtain samples of ~10 μM peptide, ~3 mM deuterated DPC, and the unbuffered pH was adjusted to ~4.8 with H₂SO₄/NaOH. Nine replicate measurements were collected over 3 separate days on a Jasco J-810 spectropolarimeter (Easton, MD) at 30 °C in a 0.1-cm path length (Hellma, Müllheim, Germany) water-jacketed cell (20 nm/min scan rate). Data were collected in a wavelength range of 260–180 nm, but the signal to noise ratio was considered reasonable only at a detector (photomultiplier tube) voltage under 700 (based on previous instrumental observation). Averaged data were analyzed by several algorithms (41) using the DICHROWEB interface (42, 43).

RESULTS

Cysteine-scanning Mutagenesis—Fig. 1A illustrates a general model of the Na⁺/H⁺ exchanger (Fig. 1A) after (11) and a schematic model of TM IX is shown in Fig. 1B. We used the cysteineless Na⁺/H⁺ exchanger (cNHE) to examine which amino acids of TM IX are critical to activity of the Na⁺/H⁺ exchanger and which amino acids are pore lining. We have shown previously that HA-tagged cNHE functions normally (16). Twenty five amino acids of TM IX (³³⁹YMA³⁶³YLSAELFHL³⁶³SGIMALIASGVVM³⁶³) were mutated to cysteine residues in the background of the cysteineless NHE1 protein. These amino acids represent more than a typical number of amino acids that cross a lipid bilayer.

Experiments examined whether these mutant forms of the Na⁺/H⁺ exchanger expressed and targeted properly and had activity. Fig. 2A shows a representative Western blot of the expression of the cysteineless NHE1, the wild type and the cysteine-scanning mutants expressed in AP-1 cells. The level of expression relative to the cysteineless Na⁺/H⁺ exchanger is shown below each mutant. Most mutants expressed to reasonable levels, greater than 60% of the values of the controls. It was notable that Y339C and S344C were mainly present as a lower molecular weight deglycosylated or partially glycosylated form.

Mutation of transmembrane amino acids can affect surface targeting of the Na⁺/H⁺ exchanger (16). Therefore, we examined intracellular targeting of the NHE1-expressing cell lines. After cells were treated with sulfo-NHS-SS-biotin, labeled proteins of lysates were bound to streptavidin-agarose beads. To

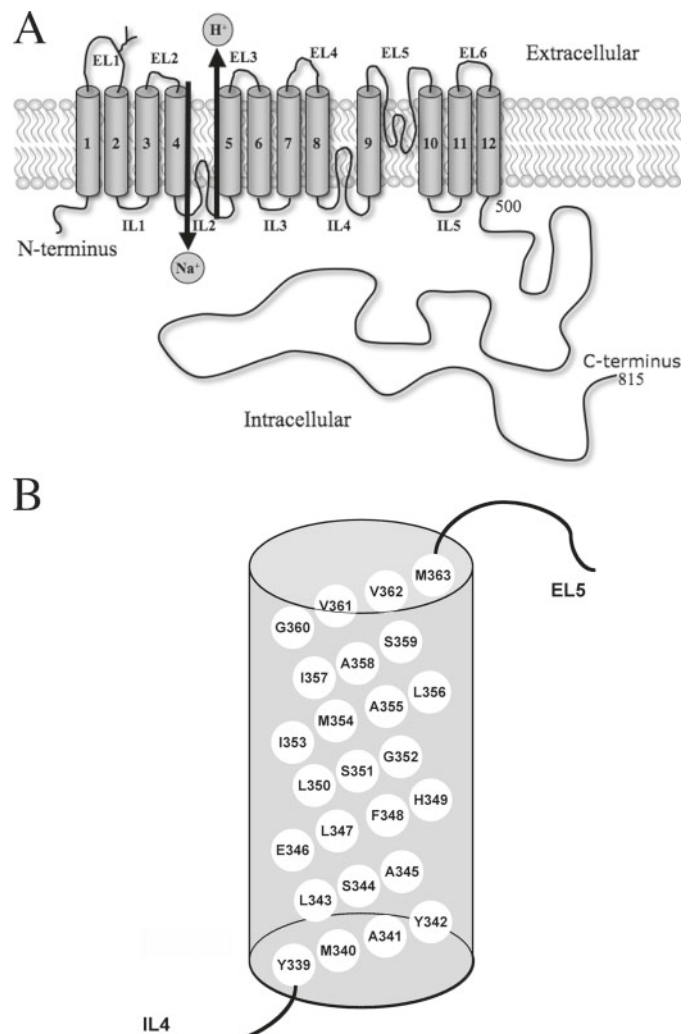


FIGURE 1. A, model of the Na⁺/H⁺ exchanger (NHE1 isoform) (11). The orientation of TM segments 1–12 of the NHE1 isoform of the Na⁺/H⁺ exchanger is illustrated. EL 1–6 and IL 1–5 refer to extracellular and intracellular loops as numbered. B, schematic model of amino acids present in TM IX.

identify NHE1 protein we used Western blotting with anti-HA antibody and examined equal amounts of total cell lysates and unbound lysates. This revealed the relative amounts of tagged intracellular NHE1 protein. Fig. 2B illustrates examples of the results and a summary of at least six experiments. Both the 110- and 95-kDa bands were included in the analysis. The results revealed that, in several cases, mutation of the amino acids to cysteine caused decreases in targeting of the protein to the plasma membrane. Most notable was the Y339C mutant that was now mostly intracellular. Most of the other mutants had reduced targeting to the cell surface by between 15 and 30%, although this still left approximately half of the protein targeting to the cell surface. Nonspecific binding of NHE1 protein to streptavidin agarose beads was ~11%, so the values shown overestimate the level of surface protein.

As part of our analysis of the effect of the mutations, we determined how the mutations of the protein affected NHE1 activity. The rate of recovery from an acute acid load induced by ammonium chloride was determined as described earlier (44). Fig. 3 illustrates an example (Fig. 3A) and a summary (Fig. 3B) of

Characterization of TM IX of the Na⁺/H⁺ Exchanger

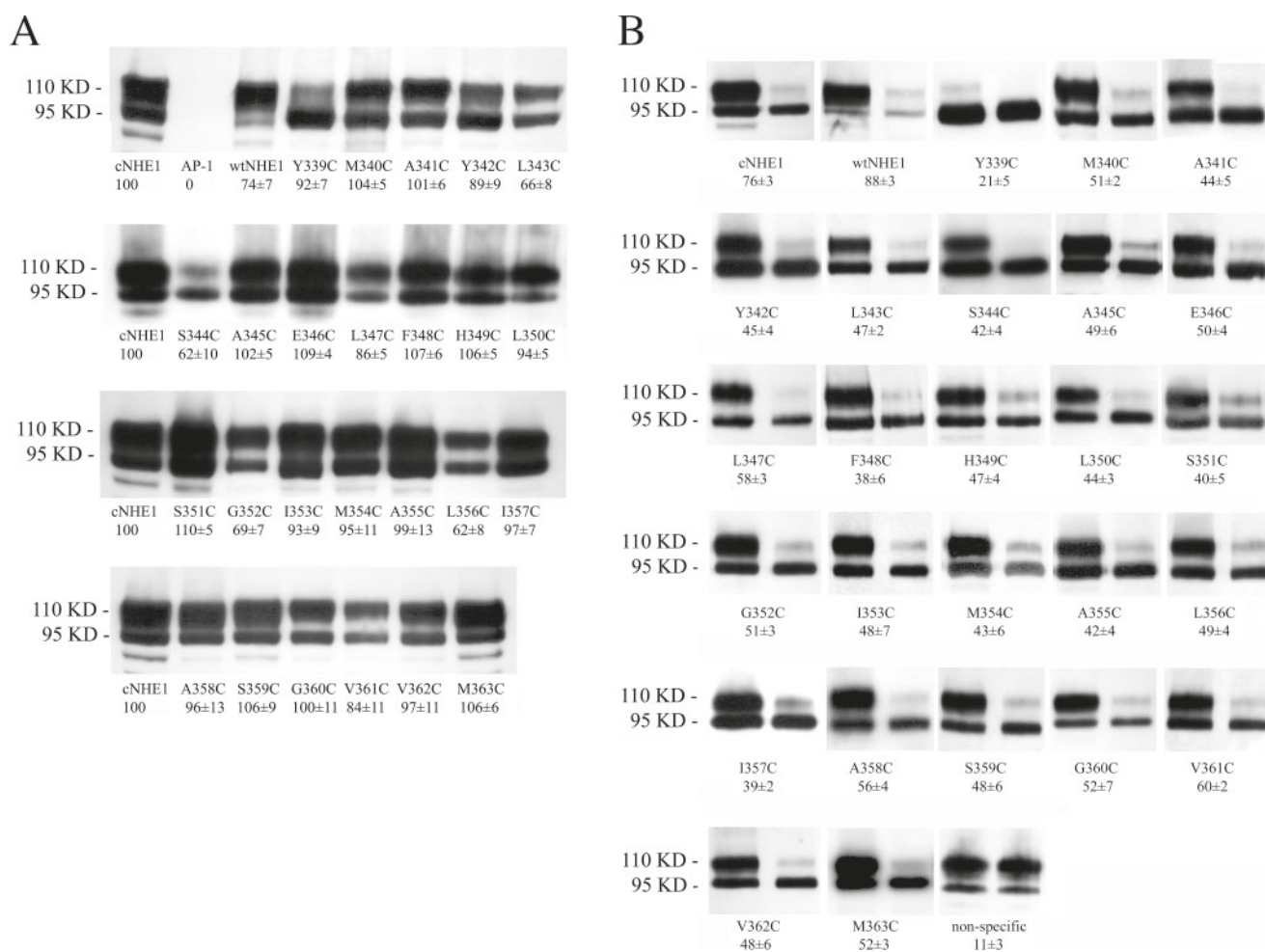


FIGURE 2. Characterization of NHE1 expression in AP-1 cells. *A*, Western blot analysis of cell extracts from control AP-1 cells and stably transfected AP-1 cells with cysteine-scanning mutations in TM IX. 100 μ g of cell extracts were prepared from control and stably transfected cell lines. Samples were examined for NHE1 expression by Western blotting versus the HA tag. Numbers below the lanes indicate the values obtained from densitometric scans of both the 110- and 95-kDa bands relative to cysteineless NHE1. Results are mean \pm the S.E. of at least three measurements. *B*, subcellular localization of control NHE1 and TM IX cysteine-scanning mutants in AP-1 cells. Cells were treated with sulfo-NHS-SS-biotin and lysed. The solubilized proteins were treated with streptavidin-agarose beads to bind labeled proteins. Equal samples of total cell lysate (*left side* of each panel) and unbound lysate (*right side*) were run on SDS-PAGE. Western blotting was done with anti-HA antibody. Nonspecific refers to an experiment in which nonspecific binding to streptavidin-agarose beads was measured by following the standard procedure without labeling cells with biotin. wtNHE1, wild type NHE1. Other mutants are as indicated. The percent of the total plasma membrane NHE1 protein that was found in each sample is indicated. The results are the mean \pm the S.E. of at least six measurements.

the rates of recovery from stable cell lines transfected with cysteineless or wild type Na⁺/H⁺ exchanger or mutants of TM IX. We also corrected the rate of recovery for both the level of expression and surface targeting so that we could determine whether the mutations affect the activity of the protein directly or indirectly through effects on trafficking and expression. Five of the mutants were severely affected by mutation to cysteine, Tyr³³⁹, Leu³⁴³, Ile³⁵³, Ala³⁵⁵, and Val³⁶¹. Correction for surface targeting and expression improved the relative activity of all these mutants slightly, although not to the level of controls. All five had less than 20% uncorrected activity compared with the cysteineless NHE1 protein. Because their low activity made further experiments impractical, these mutants were not used for any further analysis.

Sulfhydryl Modification of Cysteine Mutants—We examined the sensitivity to MTSET or MTSES of the 20 mutant Na⁺/H⁺ exchangers of TM IX that had greater than 20% residual activity of the cysteineless NHE1 (Fig. 4). MTSES caused slight, but not significant, stimulation of activity of both the wild type NHE1

and many of the mutant NHE1s (Fig. 4, *A* and *C*). Of the mutant Na⁺/H⁺ exchangers, the E346C and S351C mutants were significantly affected by treatment with the positively charged MTSET (Fig. 4, *B* and *C*). In both cases the reduction of activity was approximately 30% of the control activity. Treatment of these mutants with the negatively charged reagent MTSES did not result in significant reductions in activity. No other mutants were greatly affected by either MTSET or MTSES. However, there were minor but significant reductions in activity in two residues adjacent to the affected residues. The A345C and the L350C mutants were reduced in activity \sim 20–30%. The V362C mutant also showed a minor, significant reduction in activity.

To characterize the effect of mutation of Glu³⁴⁶ and Ser³⁵¹ in more detail, we examined the effect of the change to these amino acids on the kinetics of Na⁺/H⁺ exchanger activity. Extracellular sodium and intracellular pH values were varied, and the activity of the protein was measured, and estimates of proton affinity and V_{max} were calculated. With either mutation, both the V_{max} and the K_m values of transport were reduced (Fig.

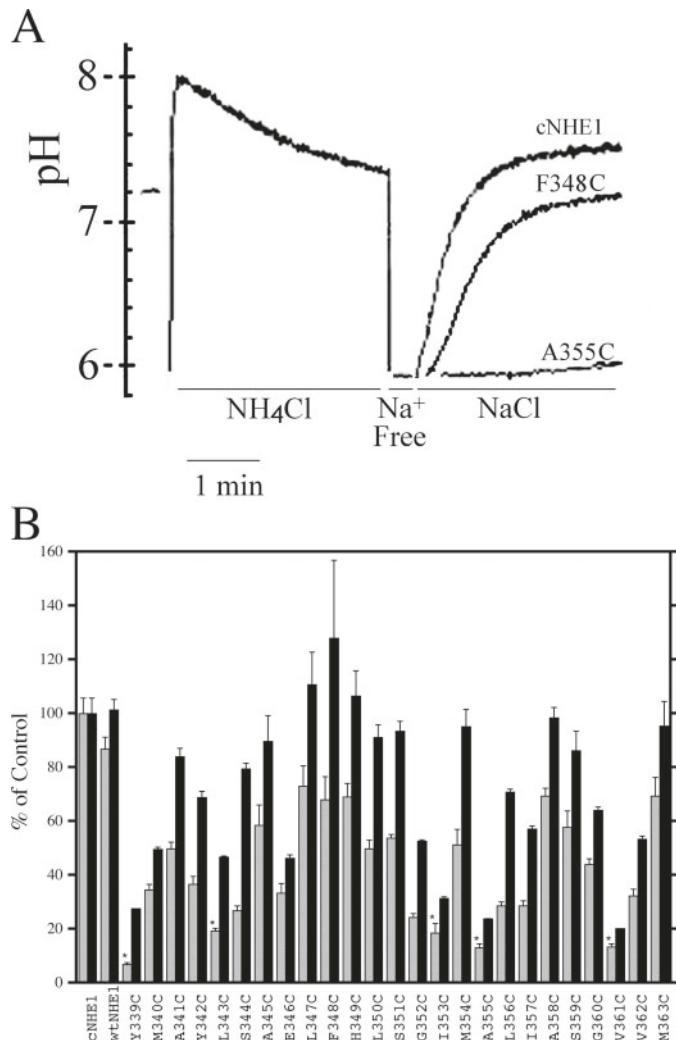


FIGURE 3. Na⁺/H⁺ exchanger activity of AP-1 cells stably transfected with cNHE1, wild type NHE1 (wtNHE1), and Na⁺/H⁺ exchanger mutants of TM IX individually changed to Cys. Na⁺/H⁺ exchanger activity was measured after ammonium chloride-induced acid load as described under "Experimental Procedures." *A*, examples of measurement of Na⁺/H⁺ exchanger activity of cNHE1, NHE1 with a F348C mutation, and NHE1 with an inactive mutation, A355C. *Bars* indicate the presence of ammonium chloride, Na⁺-free, and NaCl-containing solutions. *Traces* are shown for the entire ammonium chloride treatment and recovery of cNHE1. For clarity, only the recovery from acidosis is shown for F348C and A355C. *Lines* are slightly offset for easier viewing. *B*, summary of activity of NHE1 expressing stable cell lines. cNHE1 activity is set to 100%. All mutations were in the background of the cNHE1. All results are means ± S.E. of at least six determinations from two independently made stable cell lines. Results are shown for mean activity both uncorrected (*hatched*) and normalized for surface processing and expression levels (*solid bars*). *Asterisk* indicates mutants with uncorrected activity that is less than 20% of cNHE1.

5). When we determined the rate of proton transport of cNHE1 and the S351C and E346C mutants, we found that proton transport was greatly impaired in the mutants. The maximal rates of transport of cNHE1 and of the S351C and E346C mutants were 1.5, 1.07, and 0.12 mM/s, respectively. The activation of the mutant Na⁺/H⁺ exchanger proteins by H⁺ was also greatly impaired. Wild type NHE1 was half-maximally activated at approximately pH 7.2, whereas the S351C mutant was activated at pH 5.7 (Fig. 5A), about a 32-fold increase in H⁺ concentration. The H⁺ affinity of the E346C mutant was so poor it was not measurable by the techniques used in our study.

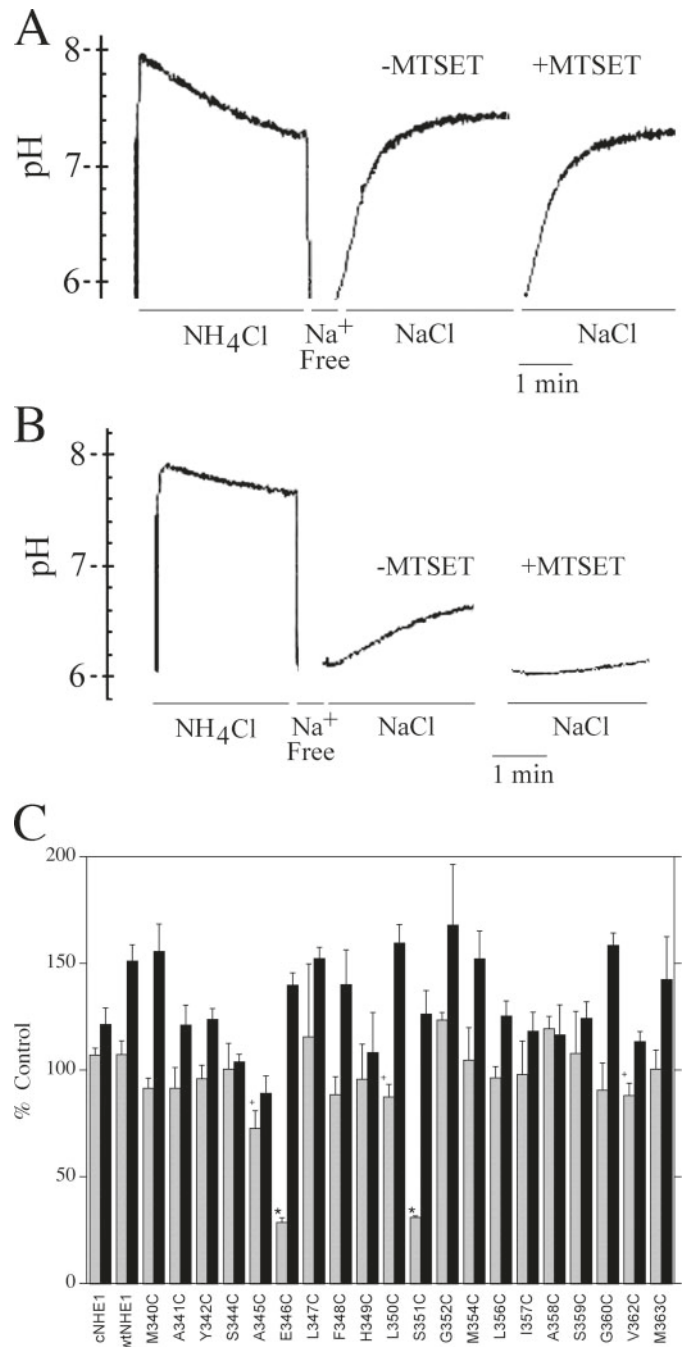


FIGURE 4. Effect of MTSET and MTSES on activity of cNHE1 and TM IX cysteine mutant NHE1 containing cell lines. Na⁺/H⁺ exchanger activity was measured after acid load as described under "Experimental Procedures." Cells were then treated with 10 mM reagent before another transient acidification. *A* and *B*, example of effect of MTSET on Na⁺/H⁺ exchanger activity of cNHE1 (*A*) and E346C NHE1 proteins (*B*). *Traces* are shown for the entire ammonium chloride treatment and recovery of cNHE1 and E346C in the absence of MTSET. For clarity, only the recovery from acidosis is shown in the presence of MTSET. *C*, summary of results that represent the % of activity after the second acid load, in comparison with the first acid load. *, + indicate that the second recovery from acid load was significantly lower in comparison with that occurring in the cysteineless NHE1, * at $p < 0.01$; + at $p < 0.05$, respectively, Mann-Whitney *U* test. *Solid filled bars* represent MTSES treatments and *striped bars* MTSET treatments.

Effects on sodium transport were also quite large (Fig. 5B). The V_{max} values for Na⁺ of cNHE1, E346C, and S351C were 0.0198, 0.0089, and 0.0109 (Δ pH/S), respectively, indicating a

Characterization of TM IX of the Na⁺/H⁺ Exchanger

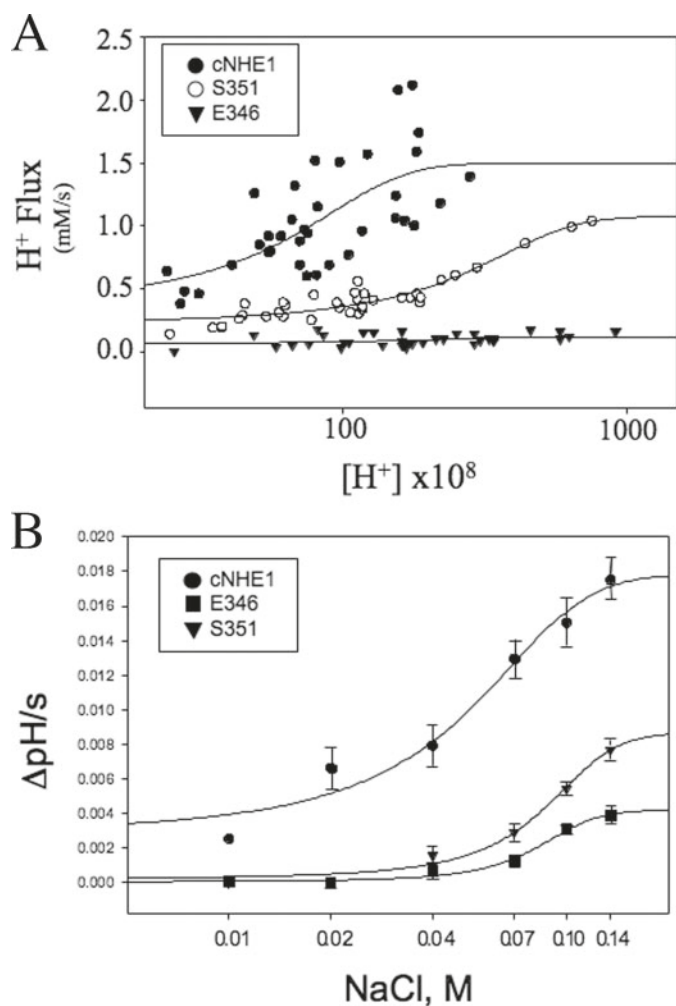


FIGURE 5. Cation affinity of wild type and mutant Na⁺/H⁺ exchangers. Na⁺/H⁺ exchanger activity of cells expressing either wild type NHE1 or NHE1 with the E346C or S351C mutations was determined as described under "Experimental Procedures." *A*, dependence of proton efflux on intracellular proton concentration. Cells were preincubated with varying concentrations of ammonium chloride for various times. Proton efflux was calculated from the initial rate of recovery times the buffering capacity. *B*, dependence of Na⁺/H⁺ exchanger activity on external sodium concentration. Na⁺ concentrations were varied while maintaining osmolarity with *N*-methyl-D-glucamine. Cells were acidified to the same degree as described under "Experimental Procedures." Results are mean ± S.E. of at least six experiments. Where not shown S.E. was too small to be displayed.

large decrease for the mutants in the maximal rate of transport. The K_m values for Na⁺ for cNHE1, E346C, and S351C were 39.3, 99.2, and 77 mM, respectively, demonstrating greatly reduced affinity for Na⁺ in both mutants.

Peptide Design and Conditions for NMR Spectroscopy—The synthetic peptide contains three lysine residues, one at the N terminus and two at the C terminus, which are not present in the endogenous sequence of the NHE1 protein. Cationic residues at the termini of peptides have been shown to facilitate both peptide purification and maintenance of transbilayer orientation (45). For convenience, the lysine residues are numbered relative to the endogenous sequence. All structural studies were conducted on the 31-residue peptide produced by chemical synthesis with no isotope labels.

Although a methanol/chloroform/water (4/4/1, v/v) mixture and dimethyl sulfoxide were both shown to solubilize the TM

TABLE 2
NMR structural statistics for the final ensemble of 40 structures retained out of 100 calculated

Average deviations are shown for XPLOR-NIH energies.

	Dihedral restraints	No dihedral restraints
Unique NOE restraints		
Total	1231	
Intra-residue	432	
Sequential	536	
Medium range $ i - j \leq 4$	238	
Long range $ i - j > 4$	2	
Ambiguous	23	
Ramachandran plot statistics		
Core	54.3%	
Allowed	34.6%	
Generously allowed	7.0%	
Disallowed	4.0%	
XPLOR-NIH energies (kcal/mol)		
Total	54.2 ± 5.6	44.8 ± 3.1
NOE	9.95 ± 2.4	8.69 ± 2.3
NOE violations		
Violations >0.5 Å	0	0
Violations of 0.3–0.5 Å	13	15
Violations of 0.2–0.3 Å	25	33

IV segment of NHE1 (16), the TM VII segment was not soluble under these or other organic solvent conditions (17). Thus, DPC micelles were employed in the latter case (17) and are also employed in this work, acting simultaneously as a solubilization medium for the peptide and as a membrane mimetic environment. Sample components were 0.9 ± 0.1 mM peptide, ~75 mM deuterated DPC, and 0.25 mM (d_6) 2,2-dimethyl-2-silapentane-5-sulfonic acid (as a chemical shift standard) in 95% H₂O, 5% D₂O adjusted to pH ~5.05 and studied at 30 °C. The peptide concentration was estimated based on ¹H one-dimensional NMR spectrum integrations relative to the internal DSS standard using assigned resonances. This temperature provided good NMR spectral characteristics, prevented precipitation for extended periods of spectroscopic study, and allows for use of the cryogenically cooled triple-resonance probe on the 800-MHz Canadian National High Field NMR Centre spectrometer. This combination of factors allowed determination of the structure of the TM IX segment in DPC micelles.

Resonance Assignment and Structure Calculation—Sequential chemical shift assignments were carried out using two-dimensional TOCSY, natural abundance ¹H-¹³C HSQC, and NOESY experiments (17, 46). Natural abundance ¹H-¹⁵N HSQC was not feasible because of low signal-to-noise arising from the tumbling rate of the peptide-containing micelles. Resonance assignments for ¹H were complete except for Met-H^ε and Phe-H^δ. In some cases there were missing or ambiguous ¹³C assignments for Tyr-C^α, Met-C^α/C^ε, Leu-C^β/C^γ/C^{δ1}, Ser-C^α/C^β, Glu-C^α, Phe-C^β, His-C^α/C^{δ2}, and Lys-C^γ. Assessment of unambiguous assignments was made as described previously (17). A total of 1231 unique NOE restraints (Table 2) were used for calculation of the TM IX structure. These are summarized graphically in terms of the standard connectivities examined for secondary structure characterization and in terms of the number of unique restraints per residue in Fig. 6.

Structural Analysis of TM IX^W Peptide—An ensemble of the 40 lowest energy structures from 100 calculated peptide structures was obtained that satisfy the 1231 observed unique NOE

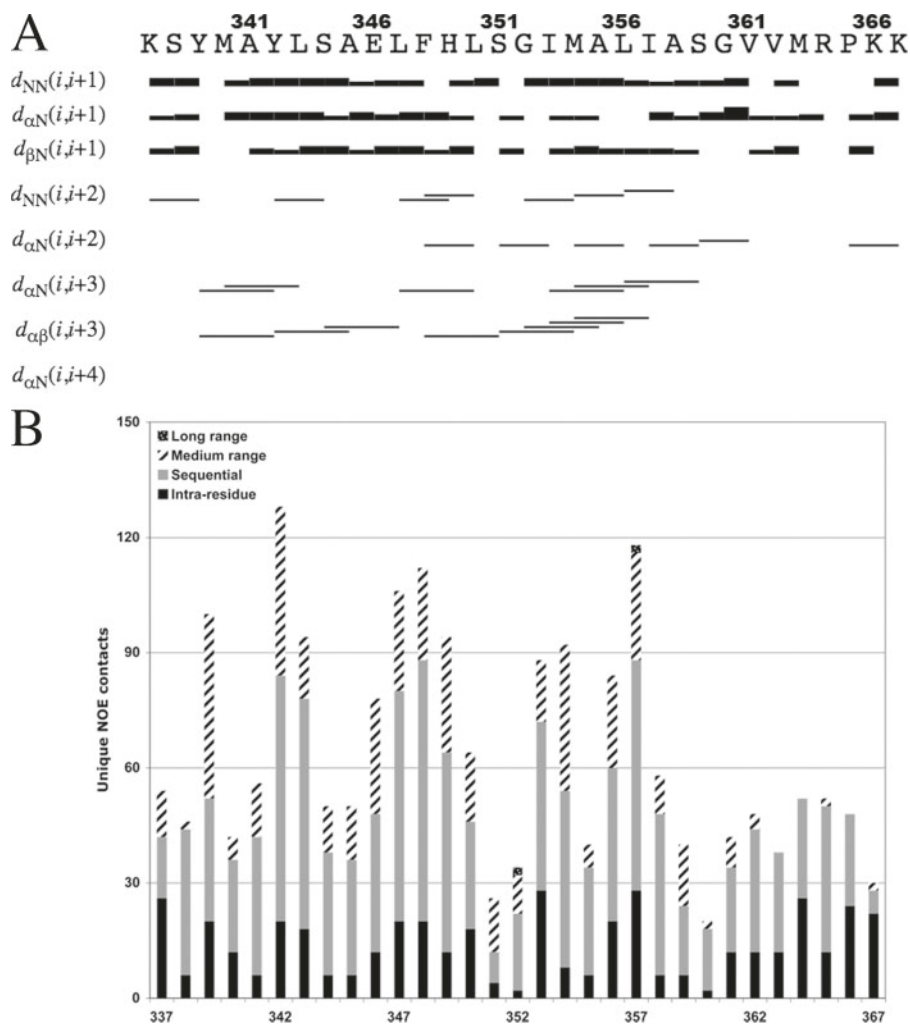


FIGURE 6. ¹H homonuclear NOE restraint assignments for TM IX in DPC micelles. These NOE restraints represent through-space interactions between nuclei that are separated by no more than ~6 Å. *A*, graphical summary of d_{xx} NOE restraints observed in the homonuclear NOESY experiment. (Figure was modified from CYANA (L.A. Systems, Inc.) output.) *B*, number of unique NOE restraints in final set of restraints on a per residue basis (medium range restraints are between nuclei 2 and 4 residues apart in sequence; long range are 5 or more residues apart).

restraints with minimal violations (Table 2). Dihedral angle restraints ($\phi = -60 \pm 30$; $\psi = -40 \pm 40$) consistent with α -helical structure were imposed over residues Met³⁴⁰–Ser³⁴⁴ and Ile³⁵³–Ser³⁵⁹. The dihedral restraints resulted in a significant but reasonable (~17%) inflation in total energy relative to an ensemble restrained only by NOEs (Table 2). The break in helicity over residues 345–352 is also consistent with secondary chemical shift data (Fig. 7A).

A 9-replicate averaged CD spectrum was analyzed using the DICHROWEB (42, 43) interface by applying several secondary structure deconvolution algorithms (results summarized in Table 3). A 190 nm low-wavelength cutoff was used for meaningful signals as detailed under “Experimental Procedures.” The normalized standard deviation parameter was used to filter those algorithms that did not produce a good fit to the data (normalized r.m.s.d. >0.2) (47). The calculated average secondary structure contributions are $26 \pm 5\%$ helix, $31 \pm 6\%$ sheet, $16 \pm 4\%$ turn, and $29 \pm 10\%$ random (Table 3). In light of the relatively high average deviations across algorithms, a qualitative inspection of the CD spectra is relevant (Fig. 8). To reflect

the 12/31 (~39%) helical residues predicted based on NMR dihedral restraints, a (theoretical) 39% helix CD spectrum from 200 to 240 nm was generated by K2D (41). The curves are qualitatively consistent with a strong helical contribution (Fig. 8).

Superposition of all members of the ensemble over the full length of the peptide was not possible. However, based on r.m.s.d. analysis as detailed in Ref. 46, Lys³³⁷–Leu³⁵⁰ and Gly³⁵²–Val³⁶² were respective N- and C-terminal segments consistent with a relatively invariant structural fold (Figs. 9 and 10). The intervening Ser³⁵¹ serves as a pivot point between the N- and C-terminal portions of the peptide, although its dihedral angles across the ensemble of structures are well clustered (Fig. 10, triangles), and its dihedral angle order parameters are close to unity, although in close proximity to a flexible region (Fig. 7B). Although residues assigned to the two helical segments were also well clustered by dihedral angle (Fig. 10, ×), there was more variability for those residues falling into superimposable regions outside of the helices proper (Fig. 10, hollow gray circles). C-terminal residues Arg³⁶⁴ and Pro³⁶⁵, which were not favored for inclusion in a C-terminal superposition, had reasonably well clustered dihedral angles in the ensemble (Fig. 10, squares). This is interesting because the preceding Met³⁶³, which was also not superimposable, had a large dispersion of backbone dihedral angles over the ensemble (Fig. 10, gray circles with dark fill).

Structural Superposition of TM IX—Peptide segments between 4 and 19 residues long were iteratively superimposed to provide a minimum r.m.s.d. relative to the backbone of the lowest energy structure (Fig. 9). Those superpositions producing the largest contiguous segment of residues with r.m.s.d. values <1.0 were additionally filtered based on average r.m.s.d. across the entire segment. The following permutations were assessed: N-terminal segments between residues 337–342 and 345–354 and C-terminal segments between residues 349–354 and 357–367 were superimposed by the method of Kabsch (48) as implemented in the LSQKAB software of the CCP4 suite (49). Lys³³⁷–Leu³⁵⁰ and Gly³⁵²–Val³⁶² were the respective N- and C-terminal regions with r.m.s.d. values most consistent with a fixed region of structure (Fig. 9, A and B). The dihedral angle order parameter (Fig. 7B) was consistent with a region of structural flexibility (e.g. a pivot point at Ser³⁵¹) between the determined segments.

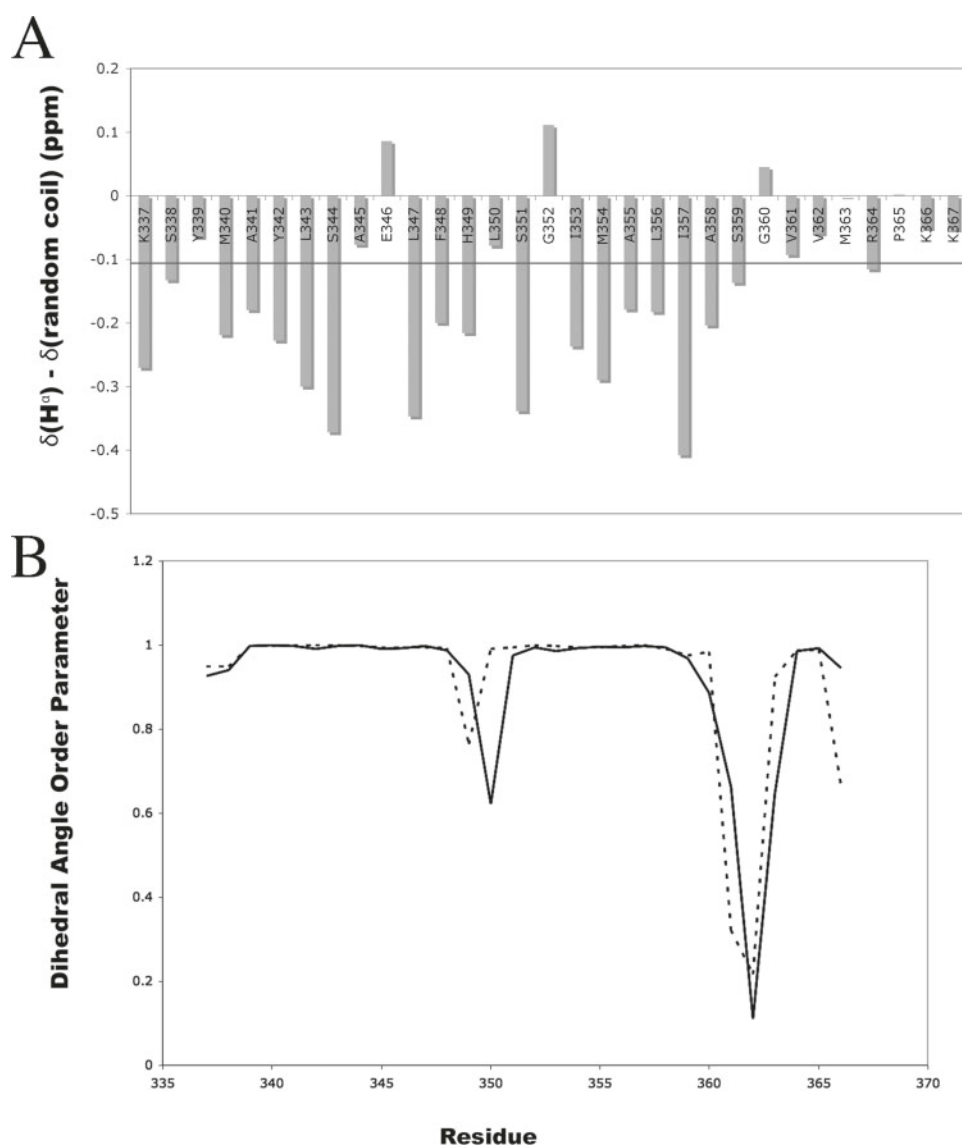


FIGURE 7. Assessment of contiguous helicity by secondary chemical shifts and dihedral angle order parameter. A, ¹H secondary chemical shifts for TM IX in DPC micelles. ¹H chemical shifts assignments from homonuclear two-dimensional NOESY (225-ms mixing time) and two-dimensional TOCSY spectra collected on an 800-MHz spectrometer. Random coil shifts (59) were subtracted from the empirical values, and the resulting secondary chemical shifts are shown for H^α. The solid line is the chemical shift difference cutoff considered significant (for helicity) for the ¹H chemical shift index (60). B, φ and ψ backbone dihedral angle order parameter for each residue of the TM IX peptide. φ (dashed line) and ψ (solid line) dihedral angle order parameters were calculated as described previously (61). Briefly, if the dihedral angle has the same value in all 40 structures of the retained NMR ensemble, its order parameter will be 1. An order parameter of 0 represents a completely random dihedral angle across the ensemble, and values 0 < order parameter < 1 represent variable dihedral angles. This parameter is used in place of the alternative measure of angular standard deviation, which does not have a defined value for truly random angles.

TABLE 3
DICHROWEB algorithm analysis of NHE1 TM IX circular dichroism spectra

A 9-replicate data set collected over 3 days was averaged in the range of 190–260 nm and used for the analysis. Only sum total contributions from each type of secondary structure are shown, even for those algorithms that estimate the number of segments of a given secondary structure (63). Average deviations are shown for average values.

Algorithm	Protein reference data base	Helix	Sheet	Turn	Random	Total	Normalized r.m.s.d.
		%	%	%	%	%	
K2D	None ^a	30	14	N/A	55	99	0.167
CDSSTR	4	21	34	20	25	100	0.018
CDSSTR	7	22	38	20	19	99	0.016
CDSSTR	SP175 (64)	19	39	8	33	99	0.021
CONTIN-LL	4	31.2	29.9	15.0	23.9	100.0	0.196
CONTIN-LL	7	31.7	31.5	16.9	20.0	100.1	0.196
Average		26 ± 5	31 ± 6	16 ± 4	29 ± 10	102	

^a K2D is a neural network algorithm that does not directly require a reference protein data base.

DISCUSSION

When we replaced amino acids of TM IX with cysteines, we found that TM IX was less sensitive than TM IV to these alterations. For TM IV, 11 of the 23 cysteine mutants had less than 20% of the activity of the control cNHE1 (16). For TM IX this only occurred in 5 instances out of 25. These results confirm our suggestion (16) that the susceptibility to mutation appears to vary not only between proteins but also within different transmembrane segments of the same protein. This was noted earlier with the lactose permease (50). The property could be reflective of both the importance of the residues in the particular segment, and of the importance of the segment itself to the structure and function of the protein. Some but not all of the amino acids of TM IX were strictly required. All the mutants of TM IX resulted in some decreases in activity that were usually caused by effects on targeting and expression levels. This suggests an important, but not essential, function of these side chains.

Structural Analysis of TM IX—Where the full-length structure of proteins is available, studies have shown that isolated transmembrane segments both reflect the structure of intact proteins and often retain their functional characteristics. Specific examples include bacteriorhodopsin (31, 32), rhodopsin (33), the cystic fibrosis TM conductance regulator (34, 35), and the fungal G-protein-coupled receptor Ste2p (51). Stabilization of the physiologi-

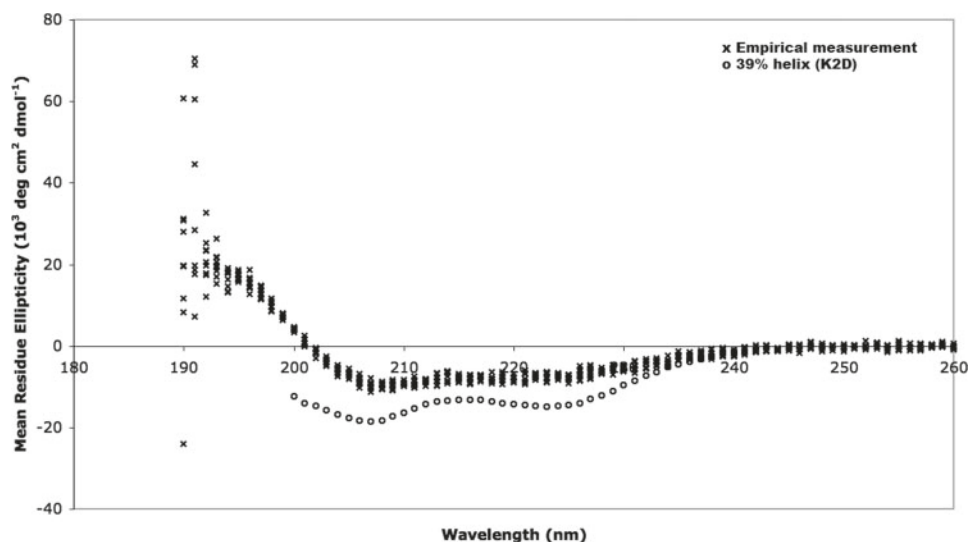


FIGURE 8. **Circular dichroism spectra for the TM IX peptide in DPC micelles.** CD samples were prepared by serial dilution of the NMR sample while maintaining DPC at a concentration of 3 mM, which is considerably greater than the critical micelle concentration of DPC ($\text{CMC}^{\text{DPC}} \sim 1 \text{ mM}$) (62). No additional UV-absorptive ions were added to the mixture. Data were collected between 260 and 180 nm and are plotted where the signal/noise was significant ("Experimental Procedures"). For comparison, the empirical data are plotted relative to a theoretical 39% helix spectrum generated using the K2D algorithm (41). Protein concentrations used for mean residue ellipticity (MRE) calculations are estimations based on integration of the one-dimensional ¹H NMR spectrum relative to the DSS internal standard.

cal structure of a TM segment may be solvent-dependent as observed previously with bacteriorhodopsin (31, 32), and TM IV (16) and TM VII (17) of NHE1. For this reason, we solubilized the 31-residue synthetic TM IX peptide in membrane-mimetic DPC micelles, a system that has been well established (36, 37). We found that the structure of the TM IX peptide in DPC micelles is an interrupted helix with a sharp, although potentially flexible, bend immediately N-terminal to Ser³⁵¹ (Fig. 9C). This bend results in a kinked, "L"-shaped structure retained across amino acids 338–365. The relative position for the N- and C-terminal superposition segments around the Ser³⁵¹ pivot is slightly variable across the ensemble. We have previously reported a similar observation for NHE1 TM VII in DPC micelles, which was also determined by NMR spectroscopy to be an interrupted helix, although with more variability in the angle of the bend between converged segments (17). The residues involved in the kink of TM VII were observed to be functionally critical residues. Similarly, we demonstrated earlier that helix IV of NHE1 is kinked at functionally important amino acids (16). The actual degree of flexibility in the context of the full-length protein would depend on constraining interactions arising from other helices, from the surrounding lipid bilayer, and through homodimer contacts (52). Kinked helices are thought to play an important role in transport function for the prokaryotic Na⁺/H⁺ exchanger NhaA (12), and the trend of our studies on TM segments of NHE1 shows residues appearing at kinked locations that are functionally critical.

There are two different membrane-spanning topologies for the NHE1 protein proposed in the literature. The first, by Wakabayashi *et al.* (11) (Fig. 1), is based on cysteine-scanning accessibility analysis and led to the present widely used model with TM IX including amino acids 338–360. More recently a model was developed based on fold recognition using the *E. coli* NhaA

crystal structure as a template for phylogenetic analysis and homology modeling (13). In this model, amino acids 338–360 of TM IX correspond to part of TM VII, a subsequent extracellular loop, and all of TM VIII. Landau *et al.* (13) suggest that the previously described TM IX is an artifact of the window size used for hydrophathy analysis. However, the TM VIII arising from their model has a membrane-spanning length of $\sim 19 \text{ \AA}$, which is short for a eukaryotic membrane (53).

Structure-Function Correlation—In all cases, we were able to express an intact Na⁺/H⁺ exchanger protein. However, five of the mutants had decreased NHE1 protein activity. For Leu³⁴³ and Ser³⁵¹ this was due, at least in part, to decreased expression and improper targeting. For Tyr³³⁹, Ile³⁵³, Ala³⁵⁵, and Val³⁶¹, significant defects in protein function were introduced by mutation.

The Glu³⁴⁶, Ile³⁵³, and Val³⁶¹ side chains face the opposite direction of Tyr³³⁹, Ser³⁵¹, and Ala³⁵⁵ side chains (Fig. 9C) in our structure. This would seem to conflict with their importance in function; however, Landau *et al.* (13) suggested that Ser³⁵¹ faces the lipid bilayer despite its functional importance and that it can rotate by 180° to face the pore for ion coordination. If true, the segment may sometimes face the pore and sometimes the lipid bilayer.

Only two mutants, Glu³⁴⁶ and Ser³⁵¹, were strongly inhibited by reaction with MTSET, and no mutants were inhibited by MTSES. The most likely explanation for their reactivity with MTSET is an interaction at a site that lines and blocks the ion translocation pore (54). There were minor inhibitory effects of MTSET on the adjacent amino acids Ala³⁴⁵ and Leu³⁵⁰ (Fig. 4C). Their mutation could cause a minor perturbation of the structure of TM IX in this region that affects Glu³⁴⁶ and Ser³⁵¹ but is also consistent with these residues having at least partial exposure to the pore. In support of this concept, Ala³⁴⁵, Glu³⁴⁶, and Leu³⁵⁰ all cluster with side chains on the same face of the segment throughout the ensemble of structures. Although Ser³⁵¹ is consistently (37/40 ensemble members) on the opposite face of the peptide, this observation may be explained by the rotation mechanism suggested by Landau *et al.* (13).

Positively charged MTSET but not negatively charged MTSES inhibited NHE1 activity in the E346C and S351C mutants. This contrasts with our results for the F161C mutant of TM IV that was inhibited by both compounds (16) but mirrors results with TM VII (55). MTSET may disrupt cation transport by direct electrostatic repulsion, whereas negative MTSES would not. Alternatively, MTSES may not be able to react with these amino acids because of repulsion on the protein surface from negatively charged amino acids important in ion coordination (56). Local protein conformation and chemistry have

Characterization of TM IX of the Na⁺/H⁺ Exchanger

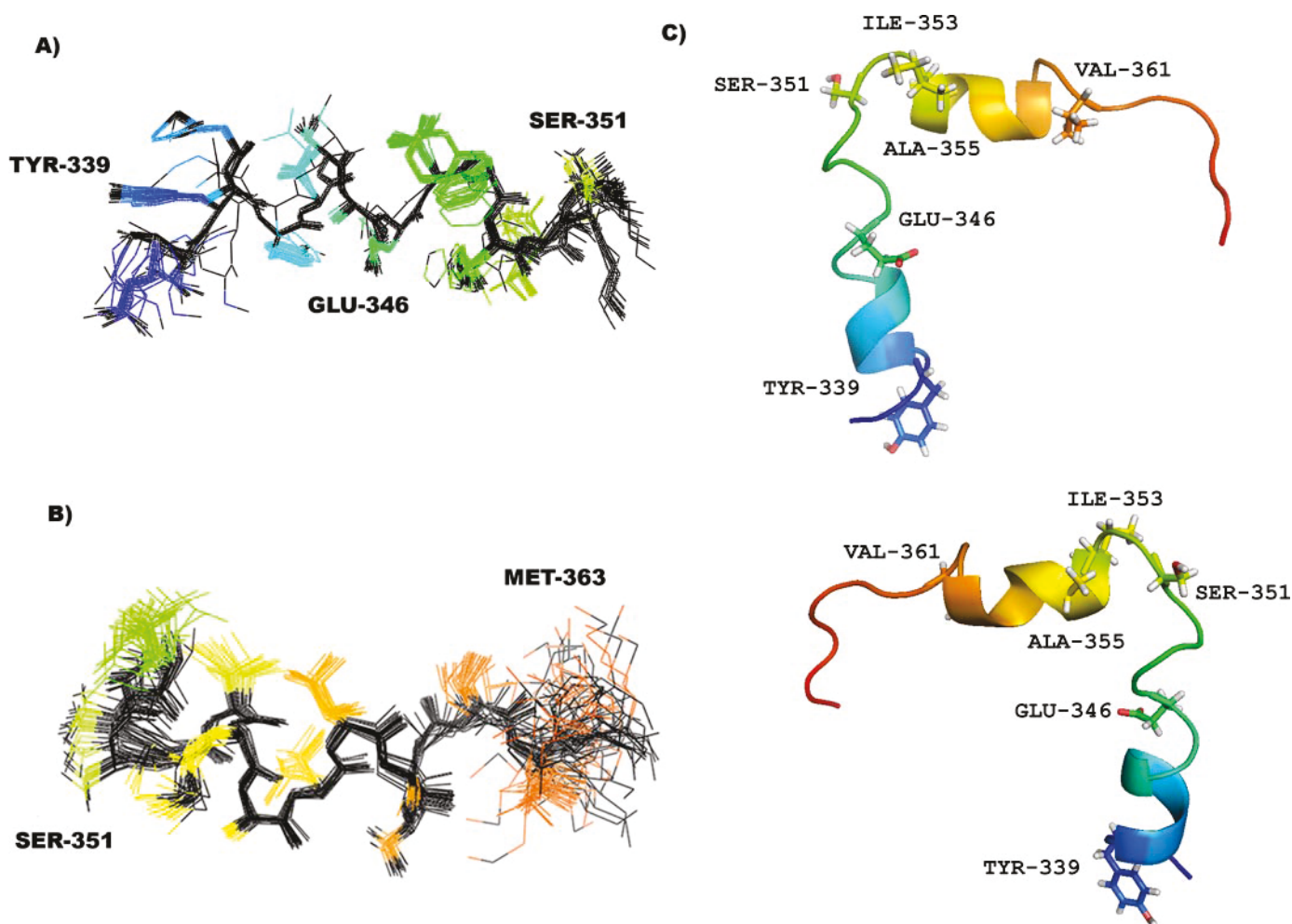


FIGURE 9. Representative and superimposed NMR structures of the synthetic NHE1 TM IX peptide in DPC micelles. Following 27 rounds of structure calculations in XPLOR-NIH (40), superpositions along the length of the 31-residue peptide structure were conducted with the LSQKAB program of the CCP4 suite (49). Optimal superposition length was determined based on iterative analysis of per residue and sum total r.m.s.d. values for several superpositions. *A*, N-terminal superposition between Lys³³⁷ and Leu³⁵⁰ over the 40/100 retained structures in the final NMR ensemble. Functionally relevant mutations in the converged 14 amino acid segment include Y339C, E346C-MTSET, and S351C-MTSET. These residues are labeled, and the structure has been extended beyond the superposition to include the pivot point at Ser³⁵¹. *B*, C-terminal superposition between Gly³⁵² and Val³⁶² in the final NMR ensemble. The pivot point residue Ser³⁵¹ is labeled N-terminal to the superposition, and the highly variable Met³⁶³ (Fig. 10) is also highlighted C-terminal to the superposition. *C*, representative structure of TM IX peptide. Two different orientations of the lowest energy ensemble member are shown on the *right* with coloring covering the spectrum from *blue* (N terminus) to *red* (C terminus). The ensemble of structures shows a slight variety of bend angles for the N- and C-terminal superposition segments about Ser³⁵¹; side chain positions are also slightly variable.

been shown to affect accessibility to sulfhydryl-reactive reagents in both K⁺ channels (57) and in the FMRF-amide-activated sodium channel (58). The E346C cNHE1 mutant exhibited a higher degree of kinetic inhibition for the same measured parameters as S351C (Fig. 5) and was similarly affected by MTSET (inhibition) and MTSES (no inhibition). In both topology models (11, 13), Ser³⁵¹ is located in the intramembrane region of the protein. Therefore, our results are consistent with Ser³⁵¹ being pore-lining in both cases and MTSET obstructing the pore. In the first topology model (11), Glu³⁴⁶ is also in the intramembrane region and should be pore-lining, potentially on the same face of a TM segment as Ser³⁵¹. However, our structural analysis did not place these residues on the same face, only 3/40 ensemble members show this positioning. This may suggest an extracellular loop position for Glu³⁴⁶, as proposed by Landau *et al.* (13). MTSET modification could then obstruct cation transport by preventing entry to the pore (Glu³⁴⁶).

The observed increase in $K_{m(\text{Na}^+)}$ for S351C mutants is consistent with at least moderately reduced extracellular coordination efficacy (Fig. 5), and may therefore be supportive of a role in the extracellular cation funnel for Ser³⁵¹ as suggested by Landau *et al.* (13). The decrease in $V_{\text{max}(\text{Na}^+)}$ may imply a measurable contribution to inhibition by a perturbation in overall pore structure or that ion coordination by Ser³⁵¹ is rate-limiting (*i.e.* that we are not simply observing reduced electrostatic interaction that can be overcome by ligand saturation). Finally, the reduced V_{max} values for H⁺ transport and especially the reduced intracellular (*i.e.* allosteric) activation of S351C cNHE1 by H⁺ are in agreement with an overall perturbation in tertiary structure (Fig. 5).

Based on dihedral restraints and r.m.s.d. analysis, our data suggest that Met³⁴⁰–Ser³⁴⁴ is helical, and although this is consistent with these residues lining a TM segment as they do in both models, the lack of contiguous α -helical character observed in the ensemble C-terminal to this segment until the

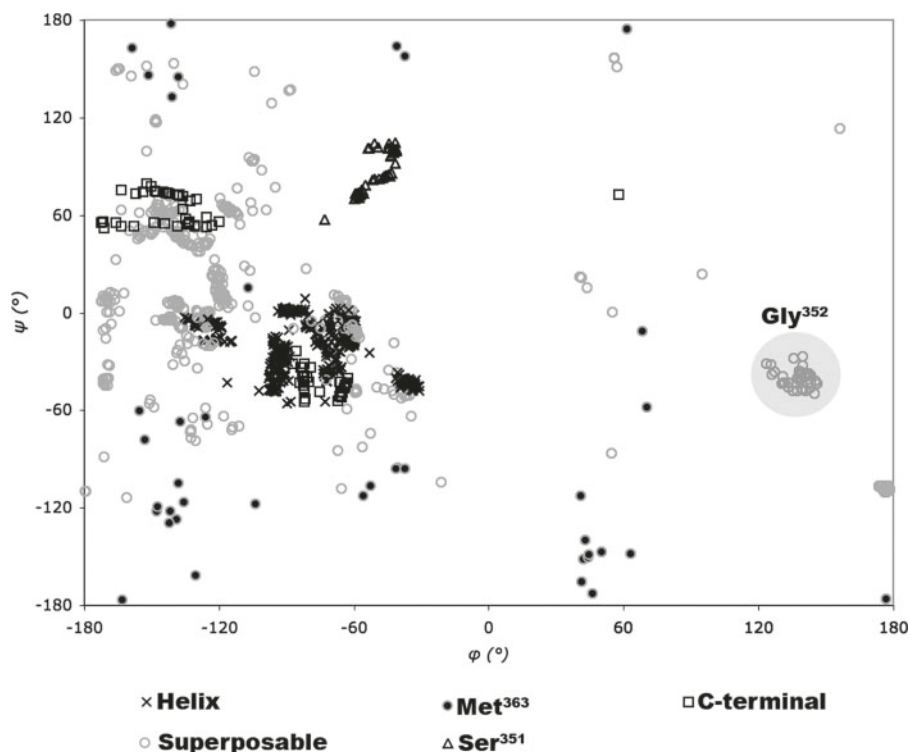


FIGURE 10. Ramachandran plot for entire retained ensemble (40/100) of TM IX peptide structures. Dihedral angle restraints ($\phi = -60 \pm 30$; $\psi = -40 \pm 40$) consistent with helical geometry (Fig. 7A) were applied in the final six cycles of structure calculation. To conservatively estimate the length and number of helical secondary structure segments, the application of dihedral restraints was iteratively varied to minimize energy computed by XPLOR-NIH (40). Residues are highlighted as helical (\times) or superimposed (hollow gray circle). The Ser³⁵¹ pivot point is indicated by triangles. The clustering of C-terminal residue angles (squares) is also compared with the Met³⁶³ dihedral angle distribution (gray circle with dark fill). The well clustered Gly³⁵² is highlighted in the large gray circle.

second major helical segment (Ile³⁵³–Ser³⁵⁹) would be consistent with the extracellular loop assignment of residues 345–352 (13). The observed pivot at Ser³⁵¹ (Fig. 9C) also supports the possibility of an adjacent flexible extracellular loop at the location suggested by Landau *et al.* (13). Glu³⁴⁶ and Gly³⁵² have been implicated as being critical in NHE1 inhibitor binding (20, 21). Placement of these residues at or near the extracellular surface is consistent with a site of drug interaction. A distorted and interrupted helix with a bent TM L-shape would result if the peptide NMR structure were applied as a single transmembrane segment (11). The bent structure we observe is consistent with a eukaryotic membrane span, the distance between C α of Ser³³⁸ and Ser³⁵⁹ is 28 ± 2 Å in our structures. Conversely, if the Landau *et al.* (13) topology is correct, residues His³⁴⁹ and Val³⁶² would be at the extracellular and intracellular faces, giving a transbilayer length of 19 ± 1 Å, a length typically assumed to be insufficient to span a eukaryotic membrane (53). To attempt to resolve these topological issues, a series of experiments were done with amino acids 345–348 to determine the accessibility to the extracellular surface. However, it was not possible to get consistent results that either verified or disproved their extracellular or transmembrane location (not shown). Even when externally accessible residues are detected, they are sometimes assigned intracellular locations using the argument that they represent pore-lining residues (11), making assignment of location somewhat arbitrary. Our functional studies showing inhibition by MTSET or our structural studies on the isolated TM

IX peptide provided valuable data on the importance of these residues in function, but they are unable to shed light on their precise topology.

We found that amino acid Met³⁶³ displayed an elevated dispersion of backbone dihedral angles, and this may suggest functionally important flexibility at this position (Fig. 10). However, our results also showed that the M363C mutation did not eliminate activity (Fig. 3B) and that it did not react with MTSET or MTSES, which is somewhat contradictory to the idea that it is critical to function. Wakabayashi *et al.* (11) suggested that M363C is in an extracellular loop. Landau *et al.* (13) placed Met³⁶³ in an intracellular loop. Our results strongly support Met³⁶³ as a loop residue displaying a high degree of flexibility, but they cannot localize this residue to either face of the membrane nor assign a critical pore-lining role to this amino acid.

Overall, our study gives a detailed structural and functional picture of the functionally critical amino acids 339–363 of the NHE1 isoform of the Na⁺/H⁺ exchanger. We demonstrate that 5 of 25 residues are very sensitive to mutation to cysteine, and that Glu³⁴⁶ and Ser³⁵¹ are involved in cation transport and likely line the cation pore. The ensemble of structures, representing a kinked helical peptide, is similar to that previously reported for TM VII (17), but with a larger bend angle at the pivot point, Ser³⁵¹. Amino acids Met³⁴⁰–Ser³⁴⁴ and Ile³⁵³–Ser³⁵⁹ are helical. To resolve whether amino acids 339–363 represent one transmembrane segment or parts of two, a full-length structure of NHE1 is most likely necessary. We recently overexpressed and purified the full-length NHE1 protein, and a low resolution structure has been obtained (52). Further detailed analysis of this protein may reveal its topology.

ACKNOWLEDGMENTS—We thank Caroline Xu, Raymond Ng, Melissa Rakovszky, and Bruce Stewart for their technical assistance, Drs. Stephen Bearne and David Waisman for access to CD spectropolarimeters, and the Canadian National High Field NMR Centre (NANUC) for use of the 800 MHz spectrometer. Operation of NANUC is funded by Canadian Institutes of Health Research, Natural Sciences and Engineering Research Council, and the University of Alberta.

REFERENCES

1. Karmazyn, M., Sawyer, M., and Fliegel, L. (2005) *Curr. Drug Targets Cardiovasc. Haematol. Disord.* 5, 323–335
2. Grinstein, S., Rotin, D., and Mason, M. J. (1989) *Biochim. Biophys. Acta* 988, 73–97
3. Pouyssegur, J., Sardet, C., Franchi, A., L'Allemain, G., and Paris, S. (1984)

Characterization of TM IX of the Na⁺/H⁺ Exchanger

- Proc. Natl. Acad. Sci. U. S. A.* **81**, 4833–4837
4. Shrode, L., Cabado, A., Goss, G., and Grinstein, S. (1996) in *The Na⁺/H⁺ Exchanger* (Fliegel, L., ed) pp. 101–122, R. G. Landes Co., Austin, TX
 5. Paradiso, A., Cardone, R. A., Bellizzi, A., Bagorda, A., Guerra, L., Tommasino, M., Casavola, V., and Reshkin, S. J. (2004) *Breast Cancer Res.* **6**, R616–R628
 6. Denker, S. P., and Barber, D. L. (2002) *J. Cell Biol.* **159**, 1087–1096
 7. Karmazyn, M., Liu, Q., Gan, X. T., Brix, B. J., and Fliegel, L. (2003) *Hypertension* **42**, 1171–1176
 8. Fliegel, L. (2001) *Basic Res. Cardiol.* **96**, 301–305
 9. Mentzer, R. M., Jr., Lasley, R. D., Jessel, A., and Karmazyn, M. (2003) *Ann. Thorac. Surg.* **75**, S700–S708
 10. Lang, H. J. (2003) in *The Na⁺/H⁺ Exchanger, From Molecular to Its Role in Disease* (Karmazyn, M., Avkiran, M., and Fliegel, L., eds) pp. 239–253, Kluwer Academic Publishers, Boston
 11. Wakabayashi, S., Pang, T., Su, X., and Shigekawa, M. (2000) *J. Biol. Chem.* **275**, 7942–7949
 12. Hunte, C., Screpanti, E., Venturi, M., Rimon, A., Padan, E., and Michel, H. (2005) *Nature* **435**, 1197–1202
 13. Landau, M., Herz, K., Padan, E., and Ben-Tal, N. (2007) *J. Biol. Chem.* **282**, 37854–37863
 14. Slepko, E. R., Chow, S., Lemieux, M. J., and Fliegel, L. (2004) *Biochem. J.* **379**, 31–38
 15. Murtazina, R., Booth, B. J., Bullis, B. L., Singh, D. N., and Fliegel, L. (2001) *Eur. J. Biochem.* **268**, 4674–4685
 16. Slepko, E. R., Rainey, J. K., Li, X., Liu, Y., Cheng, F. J., Lindhout, D. A., Sykes, B. D., and Fliegel, L. (2005) *J. Biol. Chem.* **280**, 17863–17872
 17. Ding, J., Rainey, J. K., Xu, C., Sykes, B. D., and Fliegel, L. (2006) *J. Biol. Chem.* **281**, 29817–29829
 18. Orlowski, J., and Kandasamy, R. A. (1996) *J. Biol. Chem.* **271**, 19922–19927
 19. Wang, D., Balkovetz, D. F., and Warnock, D. G. (1995) *Am. J. Physiol.* **269**, C392–C402
 20. Khadilkar, A., Iannuzzi, P., and Orlowski, J. (2001) *J. Biol. Chem.* **276**, 43792–43800
 21. Noel, J., Germain, D., and Vadnais, J. (2003) *Biochemistry* **42**, 15361–15368
 22. Mattson, G., Conklin, E., Desai, S., Nielander, G., Savage, M. D., and Morgensen, S. (1993) *Mol. Biol. Rep.* **17**, 167–183
 23. Yan, R. T., and Maloney, P. C. (1995) *Proc. Natl. Acad. Sci. U. S. A.* **92**, 5973–5976
 24. Slotboom, D. J., Konings, W. N., and Lolkema, J. S. (2001) *J. Biol. Chem.* **276**, 10775–10781
 25. Doering, A. E., Nicoll, D. A., Lu, Y., Lu, L., Weiss, J. N., and Philipson, K. D. (1998) *J. Biol. Chem.* **273**, 778–783
 26. Dunten, R. L., Sahin-Toth, M., and Kaback, H. R. (1993) *Biochemistry* **32**, 12644–12650
 27. Akabas, M. H., Stauffer, D. A., Xu, M., and Karlin, A. (1992) *Science* **258**, 307–310
 28. Stauffer, D. A., and Karlin, A. (1994) *Biochemistry* **33**, 6840–6849
 29. Holmgren, M., Liu, Y., Xu, Y., and Yellen, G. (1996) *Neuropharmacology* **35**, 797–804
 30. Liu, J., and Siegelbaum, S. A. (2000) *Neuron* **28**, 899–909
 31. Hunt, J. F., Earnest, T. N., Bousche, O., Kalghatgi, K., Reilly, K., Horvath, C., Rothschild, K. J., and Engelman, D. M. (1997) *Biochemistry* **36**, 15156–15176
 32. Katragadda, M., Alderfer, J. L., and Yeagle, P. L. (2001) *Biophys. J.* **81**, 1029–1036
 33. Katragadda, M., Chopra, A., Bennett, M., Alderfer, J. L., Yeagle, P. L., and Albert, A. D. (2001) *J. Pept. Res.* **58**, 79–89
 34. Oblatt-Montal, M., Reddy, G. L., Iwamoto, T., Tomich, J. M., and Montal, M. (1994) *Proc. Natl. Acad. Sci. U. S. A.* **91**, 1495–1499
 35. Wigley, W. C., Vijayakumar, S., Jones, J. D., Slaughter, C., and Thomas, P. J. (1998) *Biochemistry* **37**, 844–853
 36. Damberg, P., Jarvet, J., and Graslund, A. (2001) *Methods Enzymol.* **339**, 271–285
 37. Henry, G. D., and Sykes, B. D. (1994) *Methods Enzymol.* **239**, 515–535
 38. Silva, N. L., Wang, H., Harris, C. V., Singh, D., and Fliegel, L. (1997) *Pflügers Archiv. Eur. J. Physiol.* **433**, 792–802
 39. Delaglio, F., Grzesiek, S., Vuister, G. W., Zhu, G., Pfeifer, J., and Bax, A. (1995) *J. Biomol. NMR* **6**, 277–293
 40. Schwieters, C. D., Kuszewski, J. J., Tjandra, N., and Clore, G. M. (2003) *J. Magn. Reson.* **160**, 65–73
 41. Andrade, M. A., Chacon, P., Merelo, J. J., and Moran, F. (1993) *Protein Eng.* **6**, 383–390
 42. Whitmore, L., and Wallace, B. A. (2004) *Nucleic Acids Res.* **32**, W668–W673
 43. Lobley, A., Whitmore, L., and Wallace, B. A. (2002) *Bioinformatics (Oxf.)* **18**, 211–212
 44. Li, X., Ding, J., Liu, Y., Brix, B. J., and Fliegel, L. (2004) *Biochemistry* **43**, 16477–16486
 45. Davis, J. H., Clare, D. M., Hodges, R. S., and Bloom, M. (1983) *Biochemistry* **22**, 5298–5305
 46. Rainey, J. K., Fliegel, L., and Sykes, B. D. (2006) *Biochem. Cell Biol.* **84**, 918–929
 47. Mao, D., Wachter, E., and Wallace, B. A. (1982) *Biochemistry* **21**, 4960–4968
 48. Kabsch, W. (1976) *Acta Crystallogr. Sect. A* **32**, 922–923
 49. Collaborative Computational Project No. 4 (1994) *Acta Crystallogr. Sect. D Biol. Crystallogr.* **50**, 760–763
 50. He, M. M., Sun, J., and Kaback, H. R. (1996) *Biochemistry* **35**, 12909–12914
 51. Naider, F., Khare, S., Arshava, B., Severino, B., Russo, J., and Becker, J. M. (2005) *Biopolymers* **80**, 199–213
 52. Moncoq, K., Kemp, G., Li, X., Fliegel, L., and Young, H. S. (2008) *J. Biol. Chem.* **283**, 4145–4154
 53. Reithmeier, R. A., and Deber, C. M. (1992) in *The Structure of Biological Membranes* (Yeagle, P., ed) pp. 337–393, CRC Press, Inc., Boca Raton, FL
 54. Tang, X.-B., Kovacs, M., Sterling, D., and Casey, J. R. (1999) *J. Biol. Chem.* **274**, 3557–3564
 55. Ding, J., Ng, R. W. P., and Fliegel, L. (2007) *Can. J. Physiol. Pharmacol.* **85**, 319–325
 56. Dibrov, P., and Fliegel, L. (1998) *FEBS Lett.* **424**, 1–5
 57. Haug, T., Sigg, D., Ciani, S., Toro, L., Stefani, E., and Olcese, R. (2004) *J. Gen. Physiol.* **124**, 173–184
 58. Poet, M., Tauc, M., Lingueglia, E., Cance, P., Poujeol, P., Lazdunski, M., and Counillon, L. (2001) *EMBO J.* **20**, 5595–5602
 59. Wishart, D. S., Bigam, C. G., Yao, J., Abildgaard, F., Dyson, H. J., Oldfield, E., Markley, J. L., and Sykes, B. D. (1995) *J. Biomol. NMR* **6**, 135–140
 60. Wishart, D. S., Sykes, B. D., and Richards, F. M. (1992) *Biochemistry* **31**, 1647–1651
 61. Hyberts, S. G., Goldberg, M. S., Havel, T. F., and Wagner, G. (1992) *Protein Sci.* **1**, 736–751
 62. Lauterwein, J., Bosch, C., Brown, L. R., and Wuthrich, K. (1979) *Biochim. Biophys. Acta* **556**, 244–264
 63. Sreerama, N., Vennyaminov, S. Y., and Woody, R. W. (1999) *Protein Sci.* **8**, 370–380
 64. Lees, J. G., Miles, A. J., Wien, F., and Wallace, B. A. (2006) *Bioinformatics (Oxf.)* **22**, 1955–1962
 65. Goddard, T. D., and Kneller, D. G. (2001) *SPARKY 3*, University of California, San Francisco

Structural and Functional Characterization of Transmembrane Segment IX of the NHE1 Isoform of the Na⁺/H⁺ Exchanger

Tyler Reddy, Jie Ding, Xiuju Li, Brian D. Sykes, Jan K. Rainey and Larry Fliegel

J. Biol. Chem. 2008, 283:22018-22030.

doi: 10.1074/jbc.M803447200 originally published online May 28, 2008

Access the most updated version of this article at doi: [10.1074/jbc.M803447200](https://doi.org/10.1074/jbc.M803447200)

Alerts:

- [When this article is cited](#)
- [When a correction for this article is posted](#)

[Click here](#) to choose from all of JBC's e-mail alerts

This article cites 61 references, 18 of which can be accessed free at <http://www.jbc.org/content/283/32/22018.full.html#ref-list-1>